The Astrophysical Journal Letters, 725:L186–L190, 2010 December 20 doi:10.1088/2041-8205/725/2/L186

OBSERVATIONAL EVIDENCE FROM SDSS FOR A MERGER ORIGIN OF THE MILKY WAY'S THICK DISK

Marion Dierickx[1,2], Rainer Klement[2], Hans-Walter Rix[2], and Chao Liu[2]
[1] Harvard College, Cambridge, MA 02138, USA
[2] Max-Planck-Institut für Astronomie, Königstuhl 17, D-69117 Heidelberg, Germany
Received 2010 September 5; accepted 2010 November 12; published 2010 December 2

ABSTRACT

We test four competing models that aim to explain the nature of stars in spiral galaxies that are well away (>1 kpc) from the midplane, the so-called thick disk: the stars may have gotten there through orbital migration, through satellite mergers and accretion, or through heating of pre-existing thin disk stars. The eccentricity distribution of thick disk stars has recently been proposed as a diagnostic to differentiate between these mechanisms. Drawing on SDSS data release 7, we have assembled a sample of 31,535 G-dwarfs with six-dimensional phase-space information and metallicities and have derived the orbital eccentricities for them. Comparing the resulting eccentricity distributions, $p(e|z)$, with these particular simulations, we find that: (1) the observed $p(e|z)$ is inconsistent with that predicted by orbital migration only, as there are more observed stars of high and of very low eccentricity; (2) simulations in which the thick disk is made predominantly through heating a pre-existing thin disk are also inconsistent, as they predict more high-eccentricity stars than observed; (3) the observed $p(e|z)$ fits well with a "gas-rich merger" scenario, where most thick disk stars were born in situ. Further modeling could explore whether the data-simulation inconsistencies found here for the first three cases actually rule out the qualitative scenarios underlying these simulations.

Key words: galaxies: individual (Milky Way) – Galaxy: evolution – Galaxy: kinematics and dynamics – Galaxy: structure

Online-only material: machine-readable table

1. INTRODUCTION

The common presence of so-called thick stellar disk components in spiral galaxies, including the Milky Way, has been established for some decades (Burstein 1978; Gilmore & Reid 1983; Yoachim & Dalcanton 2006; Yoshii 1982): the vertical distribution of stellar brightness or mass is more adequately fit with a thin–thick disk superposition, rather than with a single (thin) disk component, where the thick disk has a scale height that is typically three times larger. Thick disk stars further differ from stellar populations closer to the galactic midplane in terms of age, metallicity, and rotational velocity. Certainly in the Milky Way, thick disk stars are generally older, more metal-poor, and rotate more slowly around the galactic center (e.g., Feltzing & Bensby 2008; Reddy 2010).

There is no consensus on the origin of the thick disk. Qualitatively different scenarios for the origin of thick disks have been discussed and cast in simulations, resulting in differing chemical and kinematic properties for the thick disk stellar population. Sales et al. (2009) examined examples of these different scenarios and proposed the orbital eccentricity distribution of stars at 1–3 thick disk scale heights from the plane as a model discriminant for the case of the Milky Way. Broadly speaking, two of the four scenarios in Sales et al. (2009) presume that the thick disk stars got heated from a once thinner disk, and two explain the thick disk as a consequence of material that was deposited in the course of a minor merger.

The first of these scenarios, *radial migration*, is based entirely on internal processes, and the thick disk is created from stars migrating outward from the kinematically hotter inner regions of the Milky Way (Roškar et al. 2008; Schönrich & Binney 2009). In the second scenario, *heating*, the thick disk is predominantly the result of rapid heating of a pre-existing thin disk through one relatively massive merger event (Villalobos & Helmi 2008). In this scenario, a modest fraction of the original thin disk is preserved (Kazantzidis et al. 2008; Villalobos & Helmi 2008), and a small portion of present-day thick disk stars were formed in the satellite galaxy and are on highly eccentric orbits.

In the *accretion* scenario, thick disk stars mostly form in an external satellite galaxy that gets disrupted while on a prograde orbit near the disk plane. This can produce many properties of observed old thick disk components (Abadi et al. 2003). Finally, the *gas-rich merger* scenario is a variant of this idea, where a minor merger epoch brings gas into the galaxy from which (thick disk) stars form before the gas completely settles into a thin disk.

Analyzing four concrete models based on these scenarios, Sales et al. (2009) proposed orbital eccentricity as a comparative diagnostic. For each simulation, they made eccentricity distributions for simulated stars distant enough from the midplane to eliminate thin disk stars. They pointed out that the eccentricity distribution $p(e|z)$ differed significantly between these four scenarios (reproduced as histograms in their Figure 3).

The aim of this Letter is to compare these predictions to the observed eccentricity distribution of thick disk stars in the Milky Way, drawing on G-dwarfs from SEGUE data release 7 (DR7) with three-dimensional position and three-dimensional velocity information. At face value, this comparison favors the gas-rich merger scenario as the most important mechanism of thick disk formation. We also point out that the relationship between height, metallicity, and eccentricity of thick disk stars has great potential for more stringent data–model comparisons with existing data.

2. DATA

2.1. Sample Definition

Sales et al. (2009) calculated their diagnostic eccentricity distribution in "solar neighborhood volumes," which they devised

Table 1
Selection Criteria for SEGUE Data

Parameter	Criterion
$(g-r)_0$	$0.48 < (g-r)_0 < 0.55$
$(u-g)_0$	$0.6 < (u-g)_0 < 2.0$
$(r-i)_0$	$-0.1 < (r-i)_0 < 0.4$
Signal-to-noise ratio	S/N > 15
Absolute velocities	$\|v\| < 600$ km s^{-1} for v_x, v_y, v_z
$T_{\rm eff}$, [Fe/H]	Have valid values
log(g)	log(g) > 3.75
$E(B-V)$	$E(B-V) < 0.3$

Notes. The first three rows impose color restrictions valid for G stars. Row 4 imposes a signal-to-noise ratio higher than 15 on the detection. The fifth removes stars that are gravitationally unbound. Row 6 specifies the need for $T_{\rm eff}$ and [Fe/H] data. Row 7 imposes high-g to select dwarfs for which photometric distances can be estimated, in accordance with Yanny et al. (2009) where the authors use log(g) = 3.75 as a cutoff value. The bottom row minimizes interstellar extinction.

as cylindrical shells between two and three scale radii of the model galaxies' thin disk ($2 < R/R_{\rm d} < 3$). To reject most of the thin disk stars, they further constrained the stars to be at $1 < |z_{\rm scaled}| < 3$ ($z_{\rm scaled} \equiv z/z_0$). For the vertical thick disk scale height z_0, Sales et al. (2009) used ∼1 kpc, except for their *accretion* model, which had $z_0 = 2.3$ kpc.

It is impossible to match such a volume with any set of actual observations. Here, we draw observations mostly from the conical volume (with the Sun at its apex) that is naturally provided by the Sloan Digital Sky Survey (SDSS) North Galactic Cap survey area. Specifically, we drew up a sample of 31,535 G-dwarf candidate stars from SDSS DR7 (Abazajian et al. 2009), for which spectra were taken and spectral parameters had been devised. Our selection criteria are outlined in Table 1, and we provide the reader with the full data in Table 2 (available online only). G-dwarfs are the best-sampled spectroscopic target category in SEGUE (Yanny et al. 2009), and a good fraction of these spectroscopic targets falls into the distance range of 0.8–6 kpc that is of particular interest here.

Photometric distances (and errors) for these target stars were derived based on their ugr colors and apparent magnitudes, following the prescription of Ivezić et al. (2008) which we expect to yield systematic errors $\lesssim$5% (Klement et al. 2009). These heliocentric distances allow us to derive the distribution of heights above the plane for these stars. For the model comparison, we need a sample of stars whose distribution $p(z)$ reasonably matches $\exp(-z/z_0)$, with $z_0 \sim 1$ kpc (as in Sales et al. 2009). We found that in the range of interest, $1 < |z_{\rm scaled}| < 3$, the $p(z)$ of our sample incidentally matches $\exp(-z/z_0)$ to within 20%. Apparently, the SDSS selection function, the G-dwarf luminosity distribution, and the conical volume compensate to provide us with the appropriate height distribution.

2.2. Phase-space Coordinates

The directly observed quantities for each star are its position, photometry, proper motion, and its spectroscopic parameters, with the line-of-sight velocity and the metallicity [Fe/H] most relevant here. These quantities need to be translated into the phase-space coordinates $\vec{\mathbf{r}}$ and $\vec{\mathbf{v}}$ and their errors in the Galactocentric reference frame. This is done using conversion matrices from Johnson & Soderblom (1987), with $v_c = 220$ km s^{-1} for the circular velocity of the local standard of rest (LSR) and 8 kpc for the Sun's distance to the Galactic center. The errors for each $\vec{\mathbf{v}}_i$ were derived following Johnson & Soderblom (1987), using the radial velocity and proper motions provided in DR7 and distance measurements taken from above. Typical errors are ∼5 km s^{-1} for the line-of-sight component (Yanny et al. 2009)[3] and ∼25 km s^{-1} for each transverse component at a distance of 2 kpc. The errors for each galactocentric $\vec{\mathbf{r}}_i$ are calculated simply from the distance error under the assumption that stellar galactic longitude and latitude are known precisely. The importance of both the individual uncertainties and of possible systematic uncertainties in the distance scale or the circular velocity at the solar radius are assessed through their impact on the derived eccentricity distribution in the next section.

3. ANALYSIS

3.1. Eccentricity Estimates

In order to calculate the orbital eccentricities for each star, we need to adopt a gravitational potential. Here, we chose a simple logarithmic potential, $\Phi = v_c^2 * \ln r$, where r is the distance from the Galactic center to the star in spherical coordinates. Although for our choice of potential an analytic solution can be obtained by using a bisection algorithm,[4] we found that this approach yields much too low eccentricities for some stars that are close to their apo- or pericenters. We therefore decided to calculate eccentricities directly through orbital integration in our potential using a leap-frog integrator and 3 Gyr integration

[3] Our formal radial velocity errors obtained from the database are smaller by a factor of ∼2; however, this only has a minor effect on the spatial velocity components compared to the proper motion errors.

[4] Bisection is a robust root-finding algorithm which bisects a given interval, evaluates in which subinterval the root must lie, and repeats the process until the desired precision is reached.

Table 2
Observed and Derived Properties of Our 31,535 SEGUE Stars

MJD	Plate ID	Fiber ID	R.A. (deg)	Decl. (deg)	l	b	...
54389	2822	350	0.0083950000	25.5169980000	108.5816000000	−35.918217	...
54380	2624	325	0.0101270000	−3.8413279000	92.9073870000	−63.675873	...
54368	2803	469	0.0165850000	28.7532920000	109.5302600000	−32.778061	...
54331	2801	345	0.0184830000	25.2723450000	108.5184900000	−36.157661	...
54452	2824	387	0.0247030000	29.1872480000	109.6592900000	−32.357891	...
...	...	...	...	...	...	...	...

(This table is available in its entirety in a machine-readable form in the online journal. A portion is shown here for guidance regarding its form and content.)

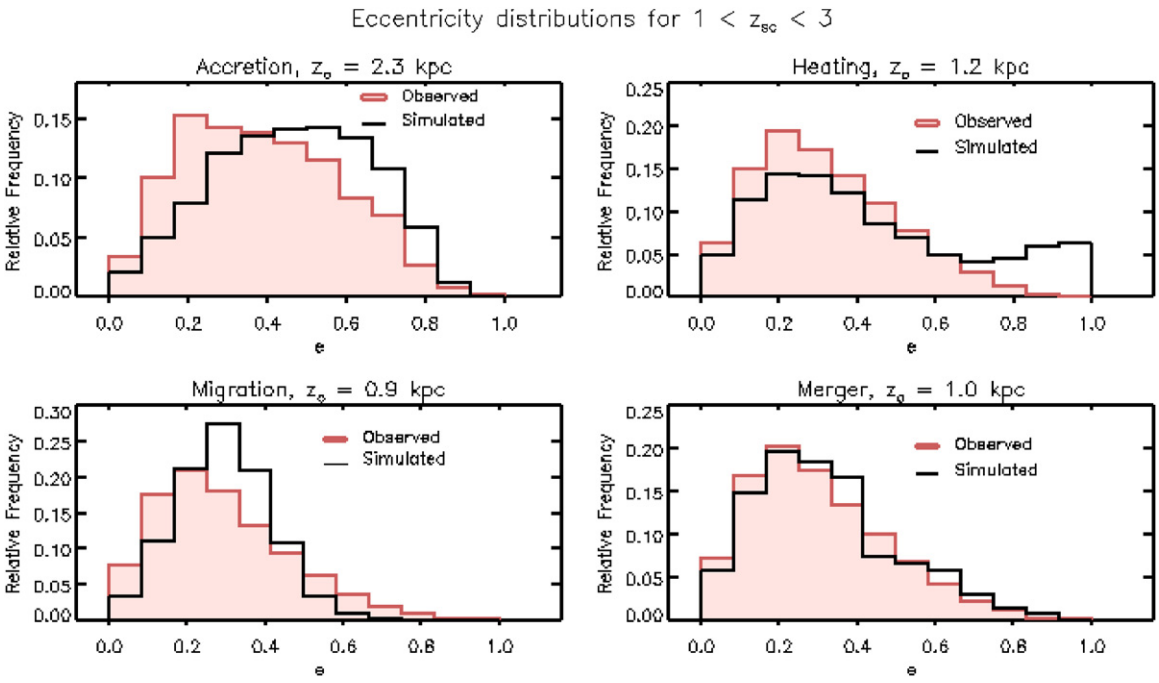

Figure 1. Eccentricity distributions for 28,377 SEGUE stars at a given height range above the midplane. The simulated data are drawn from the simulations used by Sales et al. (2009).

time. The eccentricity is then defined and given as

$$e = \frac{r_{\rm apo} - r_{\rm peri}}{r_{\rm apo} + r_{\rm peri}}. \quad (1)$$

The resulting distributions of observed orbital eccentricities are shown—as red histograms—in Figure 1, taken over height ranges $1 < |z_{\rm scaled}| < 3$.

3.2. Eccentricity Uncertainties

Before discussing these distributions, we assess the impact of two important error sources on these distributions: the individual phase-space uncertainties and the choice of the potential. For each stellar $(\vec{\mathbf{r}}, \vec{\mathbf{v}})_i$ with its associated $(\delta\vec{\mathbf{r}}, \delta\vec{\mathbf{v}})_i$, we created 100 Monte Carlo realizations of phase space coordinates, calculated the eccentricities, and created 100 realizations of the eccentricity histogram. These showed that the individual measurement uncertainties result in little variance in the eccentricity histogram and also cause no significant bias (e.g., away from small eccentricities). We also explored what the impact of a 5% systematic uncertainty in the distance (from the Sun) would be and found the effect on $p(e|z)$ to be small. We also compared $p(e|z)$ resulting from our choice of the simplistic logarithmic potential to the distribution produced by a more complex (and realistic) potential, consisting of a logarithmic halo, a Hernquist bulge, and a Miyamoto-Nagai disk (e.g., Johnston et al. 1999). The one-to-one correlation of the resulting eccentricities showed very little scatter for eccentricities less than 0.6. For higher eccentricities, the two estimates still show a good correlation, but with some net bias to larger eccentricities in the three-component potential. Adopting this more complex form for the potential would leave $p(e|z)$ largely unaffected for $e < 0.6$ and slightly boost the high-eccentricity tail. We also explored the impact of changing v_c by $\pm$ 10 km s^{-1} in the logarithmic potential context and found it to have no significant influence on the eccentricity distribution. This is because v_c enters both into the transformation to the Galactic rest frame and into the gravitational potential.

3.3. Cutting the Sample

To focus on the eccentricity distribution of thick disk stars and to minimize the contribution from the halo, we only consider stars with tangential velocity v_Φ greater than 50 km s^{-1} in the Galactocentric rest-frame system (i.e., we remove all stars on slowly rotating and retrograde orbits, consistent with Sales et al. 2009). The effect of this cutoff on the overall shape of the eccentricity distribution is negligible. We also eliminated the small fraction of stars with metallicity [Fe/H] $\leqslant -1.2$, as they may be chemically attributable to the halo (e.g., Figure 4 of Carollo et al. 2010). While this may cut out a few stars of the "Metal-Weak Thick Disk" (Carollo et al. 2010), it does not affect the overall result for the histograms in Figure 1, except for somewhat reducing the incidence of very high eccentricities ($e \geqslant 0.6$). For Figure 2, omitting the metallicity cutoff strengthens the peaks at $e \approx 0.3$–0.4 of the eccentricity distributions corresponding to the two height bins most distant from the galactic midplane. We return to the question of the correlation between kinematics and metallicity at the end, though it was not explicitly considered by Sales et al. (2009). Together, these restrictions remove 10.01% of stars in the original data set, with 28,377 stars left.

4. RESULTS

We now turn our attention to the main result of this Letter, the comparison of the observed eccentricity distributions derived from SDSS/SEGUE G-dwarfs with the model predictions by Sales et al. (2009); this comparison is summarized in Figure 1, where the panels are in the same order as in Sales et al. (2009, their Figure 3). The red histograms show the observed $p(e|z)$ for

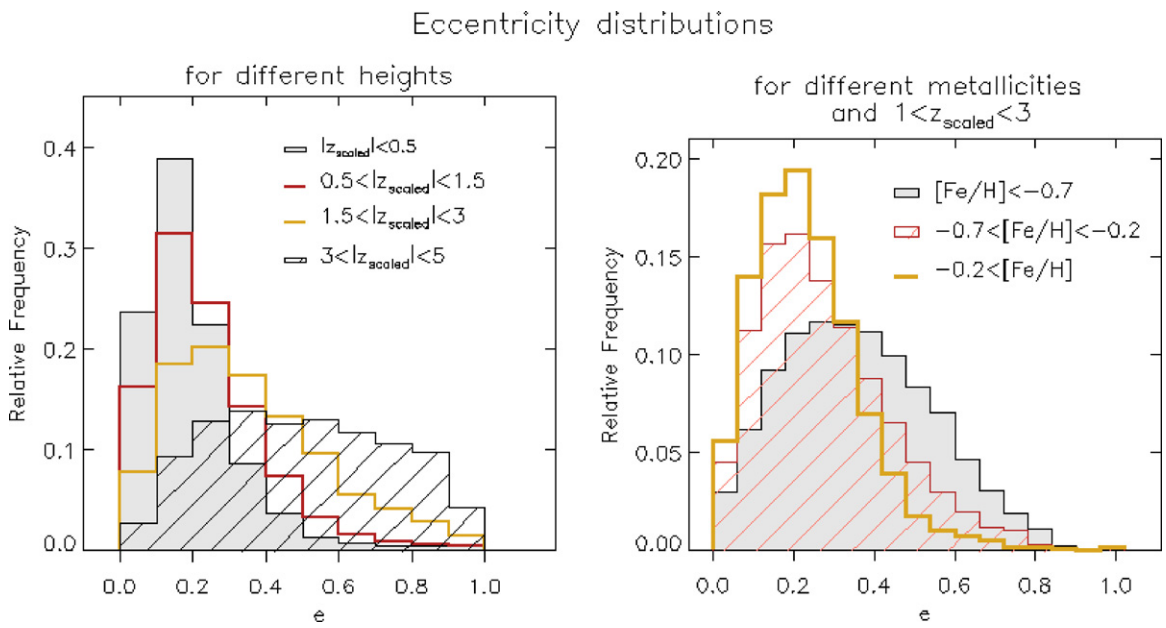

Figure 2. Eccentricity distributions for a range of heights and metallicities.

the four different scenarios, each scaled to z_0 (Table 1 from Sales et al. 2009). For all but the *accretion* scenario (top left panel) these distributions look very similar, with a peak at $e \approx 0.25$ and a pronounced asymmetric tail toward high eccentricities, $e \approx 0.9$. Unsurprisingly, for the accretion scenario the mode of the distribution is shifted toward higher eccentricities, as we sample the kinematics from 2 kpc $\lesssim z \lesssim$ 7 kpc from the disk midplane.

Figure 1 shows that neither one of the two processes where the thick disk consists predominantly of stars that were "kicked up" from a once thinner configuration matches the observed $p(e|z)$. Orbital migration (bottom left) predicts an eccentricity distribution that is too narrow. The data show a higher fraction of stars both on nearly circular and on highly eccentric orbits. The heating scenario (top right), where much of the thick disk was puffed up from a thinner disk through a massive merger, provides a reasonable match to the observations for $e \leqslant 0.6$. However, this scenario also predicts that the stars from the satellite involved in this merger should be part of the thick disk, but at very high eccentricities $0.7 < e < 1$; the data show no evidence for this. In the accretion scenario (top left) much of the thick disk consists of deposited satellite debris; as this panels shows, this predicts too high eccentricities even for the bulk of thick disk stars.

The predictions of the gas-rich merger scenario (bottom right) match the observations well, at least qualitatively if not in the formal sense: there is a maximum in $p(e|z)$ at 0.25 and a tail extending to $e = 0.9$. Recall that in this scenario both the pre-existing disk and the merging satellite are very gas-rich. Therefore, e.g., the "culprit" stars from the satellite which imply many high-eccentricity stars in the heating scenario (top right panel of Figure 1) are absent.

5. DISCUSSION AND CONCLUSIONS

We have compared the predictions made by four thick disk formation simulations to eccentricity distributions at $|z| \gtrsim$ 1 kpc resulting from SEGUE data. Eccentricity proves a valuable parameter as it allows to clearly differentiate and assess the four scenarios outlined by Sales et al. (2009). Direct accretion of stars from satellites generally predicts orbits that are too eccentric. Radial migration fails to generate the observed number of very low and very high eccentricity stars. Kinematic heating of a primordial thin disk, on the other hand, predicts too many stars with highly eccentric orbits accreted from the disrupted satellite. The accretion of gas onto the disk as a result of satellite mergers is generally consistent with the observed distribution.

Taken at face value, the comparison of the eccentricity distributions argues strongly against three of the four scenarios; they favor an origin of the thick disk ($|z| \gtrsim 1$ kpc) from a series of gas-rich (minor) mergers, where most thick disk stars formed in situ and a high-eccentricity tail arises from accreted stars. However, the simulations underlying three of the four scenarios were aimed at elucidating the physical processes capable of producing a thick disk component in late-type spirals; they were not necessarily tuned to match Milky Way properties (Brook et al. 2004; Abadi et al. 2003). Therefore, they may not represent the full range of possible $p(e|z)$ within these scenarios. Also, these scenarios are of course not mutually exclusive. For example, orbital migration must be present at some level, irrespective of the minor-merger history of the Milky Way. The bottom left panel of Figure 1 only argues against orbital migration as the sole or dominant process.

Speculation about variants of the seemingly rejected scenarios that could match the data is beyond the scope of this Letter. However, we want to point out the wealth of chemo-kinematic information that is now available to further test the origin of the thick disk. In Figure 2, we use the G-dwarf sample to illustrate how well the distribution of stellar orbits within the thick disk can be mapped as a function of height as well as metallicity: as expected, orbits become more eccentric as one moves away from the plane. At a given height above the plane, the most metal-poor stars are on the most eccentric orbits, while stars on nearly circular orbits have metallicities closer to that of the Sun (see also Ivezić et al. 2008).

Such information provides further tests of the scenarios. For example, Villalobos & Helmi (2008) find that in their thin disk heating simulation, the fractional number of accreted stellar particles increases with height above the galactic midplane. And Sales et al. (2009) argue that regardless of the specific formation

mechanism considered, accreted stars are always associated with the high-eccentricity end of the distribution.

Ultimately, the observed distributions, as, e.g., in Figure 2, should be tested against further predictions made by simulations in order to substantiate or refute gas-rich satellite mergers as a plausible thick disk formation mechanism in the Milky Way.

Funding for the SDSS and SDSS-II has been provided by the Alfred P. Sloan Foundation, the Participating Institutions, the National Science Foundation, the U.S. Department of Energy, the National Aeronautics and Space Administration, the Japanese Monbukagakusho, the Max Planck Society, and the Higher Education Funding Council for England. The SDSS Web site is http://www.sdss.org/.

M.D. acknowledges support from the Weissman International Internship Program which enabled an extended visit to MPIA, where much of this work was carried out.

REFERENCES

Abadi, M. G., Navarro, J. F., Steinmetz, M., & Eke, V. R. 2003, ApJ, 597, 21
Abazajian, K. N., et al. 2009, ApJS, 182, 543
Brook, C. B., Kawata, D., Gibson, B. K., & Freeman, K. C. 2004, ApJ, 612, 894
Burstein, D. 1978, BAAS, 10, 423
Carollo, D. A., et al. 2010, ApJ, 712, 692
Feltzing, S., & Bensby, T. 2008, Phys. Scr., 133, 014031
Gilmore, G., & Reid, N. 1983, MNRAS, 202, 1025
Ivezić, Ž., Sesar, B., Jurić, M., Bond, N., & Dalcanton, J. 2008, ApJ, 684, 287
Johnson, D. R. H., & Soderblom, D. R. 1987, AJ, 93, 864
Johnston, K. V., Zhao, H. S., Spergel, D. N., & Hernquist, L. 1999, ApJ, 512, L109
Kazantzidis, S., Bullock, J. S., Zentner, A. R., Kravtsov, A. V., & Moustakas, L. A. 2008, AJ, 688, 254
Klement, R., et al. 2009, ApJ, 698, 865
Reddy, B. E. 2010, in IAU Symp. 265, Chemical Abundances in the Universe: Connecting First Stars to Planets, ed. K. Cunha, M. Spite, & B. Barbuy (Cambridge: Cambridge Univ. Press), 289
Roškar, R., Debattista, V. P., Stinson, G. S., Quinn, T. R., Kaufmann, T., & Wadsley, J. 2008, ApJ, 675, L65
Sales, L. V., et al. 2009, MNRAS, 400, L61
Schönrich, R., & Binney, J. 2009, MNRAS, 399, 1145
Villalobos, Á., & Helmi, A. 2008, MNRAS, 391, 1806
Yanny, B., et al. 2009, AJ, 137, 4377
Yoachim, P., & Dalcanton, J. J. 2006, AJ, 131, 226
Yoshii, Y. 1982, PASJ, 34, 365